Chaos, Solitons and Fractals 209 (2026) 118540

Contents lists available at ScienceDirect

Chaos, Solitons and Fractals

journal homepage: www.elsevier.com/locate/chaos

Unstable dimension variability as a key dynamical factor shaping neural network synchronization mechanisms

Emanuel Barbosa Sant Anna Cambraia, Thiago Lima Prado, Ricardo Luiz Viana, Sergio Roberto Lopes *

Departamento de Física, Universidade Federal do Paraná, 81531-980 Curitiba, PR, Brazil
Centro Interdisciplinar de Ciência, Tecnologia e Inovação, Universidade Federal do Paraná, 81531-980 Curitiba, PR, Brazil

ARTICLE INFO

Keywords:
Neural networks
Phase synchronization
Two-state on-off intermittency
Hindmarsh-Rose neuron model
Unstable dimension variability

ABSTRACT

Neuronal network models play a crucial role in advancing our understanding of real coupled neurons and the complex dynamics that emerge from their interactions. These models make it possible to explore how connectivity patterns, coupling strengths, and intrinsic neuronal properties shape collective behaviors such as (phase) synchronization. Synchronized state stability is a key determinant of the system's long-term behavior, depending on both the intrinsic properties of the individual units and the coupling strength. In general, phase synchronization is a robust regime, but it can become fragile near critical parameter values and when it is affected by Unstable Dimension Variability (UDV) in at least one of its attractors. Here we study how UDV may be involved in the transition to a phase synchronized state of a Hindmarsh-Rose neuron-model network. We show that the level of UDV and how Lyapunov exponents oscillates around zero modifie key characteristics of the network, transforming the transition from a non-synchronized state to a phase-synchronized state originally involving bistability into an intermittent transition. We further demonstrate that, for larger coupling values, the same UDV causes the phase-synchronized state to lose global stability, leading to intermittent escapes of the trajectory from the synchronized manifold. This effect becomes stronger as the coupling increases, implying that strongly coupled networks may exhibit more phase-unsynchronized states than networks with weaker coupling.

1. Introduction

Neural network models and graph theory play a pivotal role in advancing our understanding of complex neural systems [1,2]. They are fundamental tools in understanding the complex dynamics of brain activity and neural processing [3,4]. By replicating the behavior of biological neurons and their interactions within large-scale networks, they provide valuable insights into the mechanisms underlying information transmission, emergent collective behavior, and network-level computation. Moreover, neural network dynamics are closely linked to learning [5] and memory processes [2,6], highlighting their importance in modeling cognitive function.

By employing systems of differential equations, stochastic processes, or graph-based approaches, these models help simulate the electrical activity of neurons, the propagation of action potentials, and synaptic plasticity [7]. They enable the exploration of large-scale network behavior, including synchronization, stability, and the emergence of patterns such as oscillations or chaos [8–10].

* Corresponding author at: Departamento de Física, Universidade Federal do Paraná, 81531-980 Curitiba, PR, Brazil.
E-mail address: lopes@fisica.ufpr.br (S.R. Lopes).

https://doi.org/10.1016/j.chaos.2026.118540
Received 29 January 2026; Received in revised form 11 May 2026; Accepted 15 May 2026
Available online 22 May 2026
0960-0779/© 2026 The Authors. Published by Elsevier Ltd. This is an open access article under the CC BY license (http://creativecommons.org/licenses/by/4.0/).

Furthermore, mathematical models are crucial in bridging the gap between experimental data and theoretical understanding, enabling predictions that can be tested in both computational and biological contexts [11–13].

The synchronization process in a network refers to the emergence of coherent behavior among interconnected dynamical neurons through mutual interactions [8,14,15]. As coupling strength increases or connectivity enhances, individual nodes begin to align their temporal dynamics, eventually evolving towards a common rhythm or shared trajectory. Recent studies also show an intricate relationship between synchronization and the properties of the local dynamics of the nodes of the network [16–19]. This process can occur globally, where all nodes synchronize to a single state, or partially, forming synchronized clusters that coexist with unsynchronized regions. In this way, synchronization arises from the balance between local dynamics, coupling topology, and interaction strength. In complex systems, this collective behavior enables efficient communication, coordination, and information transfer across the network.

Recent applications of neural network synchronization have expanded to encompass cutting-edge areas, such as studies in advancing the understanding of neurodegenerative brain diseases like Parkinson's and Alzheimer's [20,21], as well as neuropsychiatric disorders like schizophrenia [22].

In general, synchronization is a robust phenomenon [8]. Nevertheless, near the boundaries of stability, synchronization can become fragile, exhibiting intermittent or chaotic fluctuations that reflect the intricate interplay between individual dynamics and network structure. In some cases, the transition from unsynchronized to synchronized regimes of a network may involve hysteresis [18] and the transition from one state to another involves an explosive transition, configured as an abrupt transition from one branch to another [10,23]. In these cases, the network state depends not only on the current parameters but also on its history, meaning the system can follow different trajectories when a control parameter is increased versus when it is decreased.

Unstable Dimension Variability (UDV) may have implications for such a synchronization process associated with critical parameters and/or hysteresis. When UDV emerges, the number of unstable directions in the system fluctuates across at least one of the attractors in the hysteresis regime, leading to a loss of uniform stability of the manifold. This variability may cause intermittent episodes of desynchronization that manifest as bursts in the network dynamics, where the network temporarily loses coherence before returning to synchrony. Such behavior indicates that the network operates near a critical boundary between stable and unstable synchronization, where small perturbations can produce large, unpredictable effects. As a result, UDV introduces non-hyperbolic dynamics, making the system highly sensitive to initial conditions and numerical errors. This phenomenon may contribute to the emergence of metastable states and dynamic flexibility, allowing for transitions between synchronized and unsynchronized activity patterns that are essential for adaptive information processing and cognitive function. As the control parameter is swept, local fluctuations in stability (caused by UDV) can trigger premature switching or delayed transitions, breaking the smoothness expected in ordinary hysteresis loops.

Here, a globally coupled network of Hindmarsh-Rose (HR) neurons [12] is used to investigate the effect of UDV on the phase synchronization process of the network. The HR neuron model is a simplified version of the Hodgkin–Huxley model [11] but is able to exhibit both spiking and bursting behaviors, as well as regular and chaotic dynamics. This makes it an ideal model for exploring how local neuronal dynamics affect network-level phase synchronization, leading to a complex synchronization scenario that includes bistability, hysteresis, and intermittency behaviors [16,18,19].

Phase synchronization is quantified using the Kuramoto order parameter [24,25] which is defined from the individual neuronal phases, while UDV is quantified using the finite-time Lyapunov exponent spectrum. The text is organized as follows: In Section 2, we present the single-neuron model, together with the network coupling scheme and the synchronization quantifiers. The results are discussed in Section 3, while Section 4 is devoted to the conclusions.

2. The Hindmarsh-Rose model

2.1. Individual dynamics

Each HR neuron is described by a three-dimensional system of nonlinear differential equations that captures the membrane potential, fast current dynamics, and slow adaptation currents, enabling it to reproduce a wide range of firing patterns observed in real neurons

$$\frac{dx}{dt} = y + \phi(x) - z + I, \tag{1}$$

$$\frac{dy}{dt} = \psi(x) - y, \tag{2}$$

$$\frac{dz}{dt} = r[s(x - x_r) - z], \tag{3}$$

where the parameters a, b, c, d are associated with the fast ion channels, r and s model the slow ion channels, while $\phi(x) = -ax^3 + bx^2$ and $\psi(x) = c - dx^2$. Finally, I is the input excitatory current in each neuron. The following parameters are kept constant: $a = 1.000$, $c = 1.000$, $d = 5.000$, $r = 0.010$, $s = 4.000$, $x_r = -1.600$ and the parameters b and I are allowed to have values in the intervals: $b = [2.600, 2.700]$, $I = [4.250, 4.450]$.

The Hindmarsh–Rose neuron model holds significant physical and biological importance due to its ability to reproduce a wide range of neuronal behaviors observed in real systems while maintaining relatively low mathematical complexity [12,26,27]. Biologically, it captures essential features of neuronal activity such as spiking, bursting, and transitions between quiescent and active states, which are fundamental for information processing in the brain [26,28,29]. These dynamics are associated with real

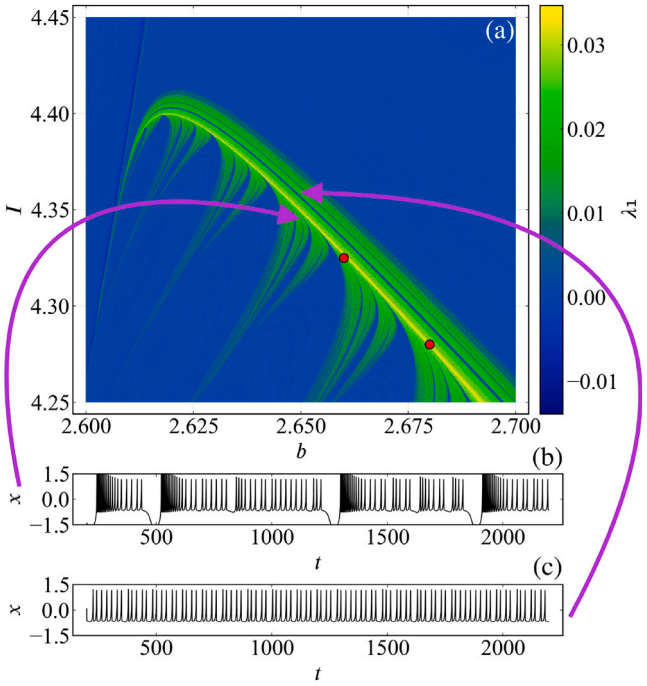


Fig. 1. Panel (a) An overview of the parameter space $b \times I$, revealing four distinct dynamical regions. The color scale (green to yellow) encodes the maximum Lyapunov exponent, with blue tones indicating zero values corresponding to periodic dynamics. On the left, the system exhibits regular bursting without chaotic intervals (to the left of the dark blue line), while the upper region is characterized by regular spiking in the absence of bursts. The lower region displays bursting dynamics interspersed with chaotic intervals (colored fingers), and the chaotic region itself is represented by colors corresponding to positive Lyapunov exponents. Notably, the chaotic domain delineates the transition between spiking and bursting behaviors. Panels (b) and (c) show representative examples of chaotic activity from the colored region as arrows indicate. The two red dots in panel (a) mark representative parameter values for the hysteresis ($b = 2.660$, $I = 4.325$) and intermittent ($b = 2.680$, $I = 4.280$) regimes analyzed in Figs. 3–7. (For interpretation of the references to color in this figure legend, the reader is referred to the web version of this article.)

electrophysiological mechanisms, including fast membrane potential changes and slower ionic currents, allowing the model to qualitatively mimic neuronal firing patterns observed in experiments [26,30].

From a physical and dynamical systems perspective, the Hindmarsh–Rose model provides a scenario for studying nonlinear phenomena such as chaos, bifurcations, multistability, and synchronization in coupled systems [27]. Its structure allows for the investigation of complex behaviors like intermittency and nonhyperbolicity, making it particularly suitable for analyzing collective dynamics in neuronal networks [19,29]. Because of its balance between biological relevance and analytical tractability, the model has become one of the standard tools for exploring how microscopic neuronal properties give rise to macroscopic dynamical patterns in large-scale brain activity [29].

An overview of the parameter space $[I \times b]$ for the isolated HR neuron model [12] is shown in Fig. 1. In general, the parameter space reveals four distinct dynamical regions. On the left side, the dynamics corresponds to regular bursting without the presence of chaotic intervals (to the left of the dark blue line). The upper region exhibits regular spiking dynamics in the absence of bursting, whereas the lower region corresponds to bursting dynamics intermingled with chaotic intervals (colored "fingers"). Finally, the chaotic region is represented by colors corresponding to the values of the maximum Lyapunov exponent, as shown in panel (a), and blue tones correspond to zero values of the maximum Lyapunov exponent [31], thus indicating periodic regimes. We set a transient time of $T_{tr} = 20$k and $T_f = 25$k as the final times of the simulations.

It is clear that the chaotic region acts as a transition zone between the spiking (upper figure areas) and bursting (lower areas) dynamics. Panels (b) and (c) illustrate two representative examples of chaotic dynamics identified in the parameter space of panel (a) by purple arrows. Panel (b) illustrates a point in the chaotic phase space of the figure located near the lower boundary, where the dynamics is bursting. Panel (c) illustrates a chaotic case in which the spiking dynamics from the upper region of panel (a) strongly influence the system's chaotic behavior. The red dots in panel (a) are representative values for the network hysteresis ($b = 2.660$, $I = 4.325$) and intermittent ($b = 2.680$, $I = 4.280$) regimes studied in detail in Figs. 3–7. Similar behaviors to these two examples can be found throughout the chaotic region.

2.2. Coupled dynamics

The HR neurons are globally coupled in a network through electrical connections, they can exhibit rich collective behaviors, including synchronization, phase locking, and complex spatiotemporal patterns.

$$\frac{dx_i}{dt} = y_i + \phi(x_i) - z_i + I + I_{i,\text{synch}}, \tag{4}$$

$$I_{i,\text{synch}} = \frac{\varepsilon}{\bar{n}} \sum_{j=1}^{N} e_{i,j} x_j(t), \ j \neq i, \tag{5}$$

where ε denotes the coupling strength parameter, and $\bar{n}$ represents the number of connections each neuron receives from the other neurons in the network. In the case of a globally coupled network, $\bar{n} = N - 1$, and all admissible elements of the coupling matrix $e_{i,j}$ are equal to one, resulting in $(N^2 - N)$ nonzero elements in total. Finally, the number of neurons in the network is $N = 200$. Our results show that this network size is adequate such that finite-size effects do not affect the observed phenomena. Simulations with networks of up to $N = 1000$ were performed to support this conclusion.

Physically, this coupling models a linear interaction mediated by the underlying network connectivity, where each node receives an input proportional to the states of its connected neighbors. The adjacency matrix defines the interaction structure, while the coupling strength controls the overall influence of the network. The normalization by the average degree ensures that the total input remains bounded and comparable across nodes, preventing highly connected units from dominating the dynamics. Such a formulation is widely used to describe synchronization phenomena, signal propagation, and the emergence of collective behavior in complex [3,4].

From a biological perspective, this coupling term can be interpreted as a synaptic input current in neuronal networks. Each neuron integrates contributions from its presynaptic partners, with the connectivity matrix encoding the synaptic architecture and the node states representing neuronal activity [1]. The coupling strength reflects synaptic efficacy, while the normalization introduces a form of balance that avoids excessive excitation in highly connected neurons. This type of interaction captures essential mechanisms such as input integration, coordinated activity, and the emergence of coherent or intermittent dynamical states, which are fundamental in brain function and neural information processing [1].

2.3. Network synchronization measures

The phase synchronization of neurons within a network can be quantified by assigning a bursting phase variable to each neuron's action potential [8].

$$\theta_j(t) = 2\pi k_j + 2\pi \left(\frac{t - t_{k,j}}{t_{k+1,j} - t_{k,j}} \right), \qquad t_{k,j} \leq t < t_{k+1,j}, \tag{6}$$

where $k_j \in [0, \text{total number of bursts}]$ denotes the burst counter, and $t_{k,j}$ is the onset time of the kth burst of the jth neuron, as defined by the dynamics in Eq. (4). Accordingly, the duration of each burst is given by $t_{k+1,j} - t_{k,j}$ [9,32]. Using Eq. (6), phase synchronization can then be quantified through the Kuramoto order parameter [24,25]

$$R(t) = \left| \frac{1}{N} \sum_{j=1}^{N} e^{i\theta_j(t)} \right|, \tag{7}$$

where $\theta_j(t)$ is the phase from Eq. (6), and $R(t) \in [0, 1]$ quantifies the degree of phase synchronization.

Associated with the definition of the oscillator phases given by Eq. (6), it is also possible to define a phase dispersion function that quantifies the collective misalignment between oscillators and vanishes at complete synchrony,

$$V(\theta(t)) = \frac{1}{N(N-1)} \sum_{(i,j)} a_{ij} \left(1 - \cos(\theta_i - \theta_j)\right). \tag{8}$$

If a harmonic variation assumption is imposed on the $\theta(t)$ phase dynamics, the condition $\dot{V} < 0$ can be obtained and a connection with a Lyapunov-type function established [33], capturing the tendency of the network to self-organize towards coherent behavior.

The $V(\theta)$ function provides a bridge between the high -dimensional neuronal dynamics and a low-dimensional description of synchronization, encoding how coupling promotes the reduction of phase disorder and stabilizes collective rhythmic activity. Nevertheless, the Lyapunov conditions ($\dot{V} < 0$) may not hold globally due to the chaotic dynamics associated with the presence of UDV of the synchronized and non synchronized attractors. For small phase differences, expanding the complex exponential from the definition of the order parameter, Eq. (7), yields the approximation

$$V(\theta(t)) \propto \left(1 - R^2(\theta(t))\right). \tag{9}$$

This establishes a direct relation between the energy-like formulation of synchronization through Eq. (8) and the statistical description provided by the Kuramoto order parameter, given by Eq. (7) [33].

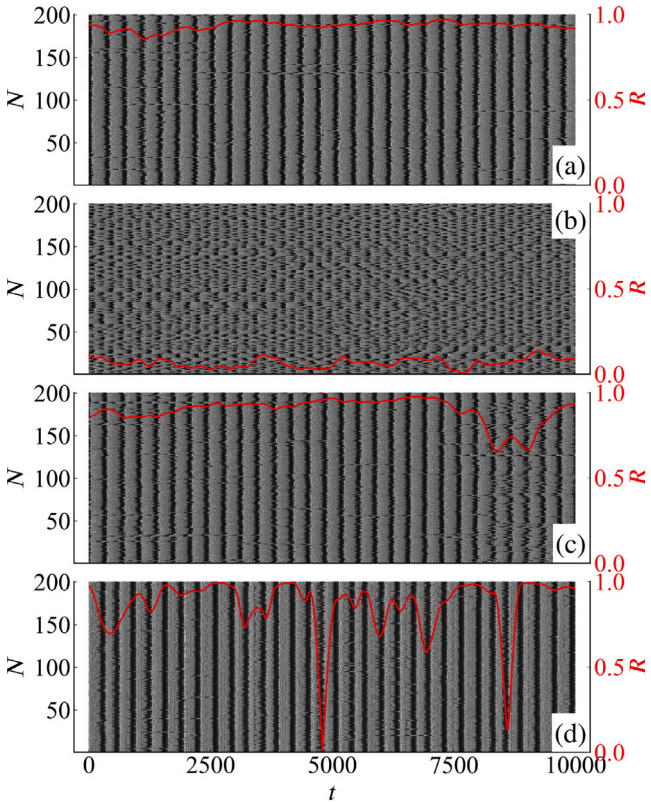


Fig. 2. Raster plot of network action potential x superposed by $R(t)$ plotted in red lines. (a) $I = 4.325$, $b = 2.660$ and $\varepsilon = 0.090$ for a synchronized basin, (b) $I = 4.325$, $b = 2.660$ and $\varepsilon = 0.090$ for a unsynchonized basin, (c) $I = 4.280$, $b = 2.680$ and $\varepsilon = 0.100$ and (d) $I = 4.325$, $b = 2.660$ and $\varepsilon = 0.500$. (For interpretation of the references to color in this figure legend, the reader is referred to the web version of this article.)

3. Results and discussions

The network of Hindmarsh–Rose neurons, for the parameter ranges shown in Fig. 1(a), exhibits four distinct regimes as the coupling strength is increased. To illustrate all these dynamical regimes exhibited by the HR neuronal network, Fig. 2 shows representative examples of the network behaviors as the coupling parameter is increased and for the two distinct points indicated by red bullets in the parameter space given in Fig. 1(a). (*i*) For coupling slightly above a critical value for the partially phase synchronized regime, the network is characterized by small excursions of the order parameter within the interval $0.8 < R(t) < 1.0$, as illustrated in Fig. 2(a); This regime coexists with a second one that remains unsynchronized, as shown in Fig. 2(b), thereby characterizing a hysteretic region in which two globally stable attractors coexist; (*iii*) For a second point in the parameter space depicted in Fig. 1(a) and for similar coupling strengths, a regime of intermittent phase synchronization occurs, indicating that the phase synchronized state is not globally stable for some points in the parameter space (Fig. 2(c)); and finally, (*iv*) for sufficiently large coupling values, a regime in which the trajectory, although influenced by the phase synchronized attractor, begins to exhibit sharp escapes from the phase synchronized dynamics, revealing a progressive loss of global stability of the phase synchronized state for large values of the coupling strength (Fig. 2(d)). In this latter regime, the attractor's stability is affected by the presence of strong UDV in the system, which gives rise to increasingly frequent and intense departures from the synchronized state.

Fig. 3 panel (a) shows the time average value of the order parameter given by Eq. (7) for increasing (black bullet curve) and decreasing (red star curve) values of the coupling strength. The black (red) curve is obtained by initializing the system with the lowest (highest) value of the coupling parameter. After the first value of $\langle R \rangle$ is computed, the coupling parameter is gradually increased (decreased), and each new trajectory is initialized using the final state from the simulation with the previous coupling value. This procedure increases the likelihood of maintaining the system in a state close to the preceding one, thereby ensuring a smooth continuation of the system towards its asymptotic regime. As observed in Fig. 3 panel (a), computed for parameter values $b = 2.660$, $I = 4.325$ corresponding to the upper red bullet in Fig. 1(a), the network exhibits bistable behavior in the gray shadow area, $(0.070 \lesssim \varepsilon \lesssim 0.115)$, in which one attractor displaying partially phase synchronized dynamics coexists with another depicting unsynchronized dynamics. In this regime, both attractors are globally stable, possessing their own basins of attraction. Panels (b) – (f) of Fig. 3 present representative examples of how $R(t)$ evolves over time for 5 values of the coupling strength. In Panels (b) – (f), red shading indicates time intervals for which $R(t) > 0.8$, corresponding to periods of partial phase synchronization among the

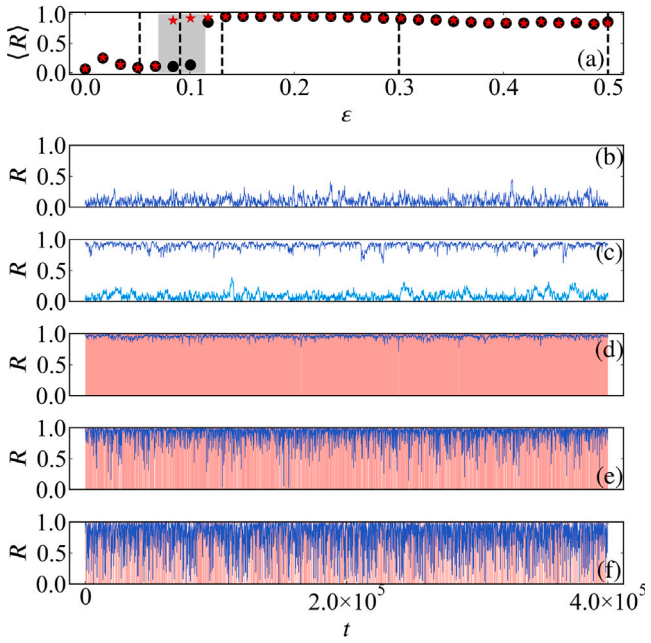


Fig. 3. (a) Mean Kuramoto order parameter $\langle R \rangle$ as a function of the coupling strength ε for $b = 2.660$ and $I = 4.325$, obtained using continuation. Black dots correspond to the forward continuation, while red stars denote the backward continuation. Vertical dashed lines mark the coupling values used in panels (b)–(f). Panels (b)–(f) show the time series of the Kuramoto order parameter $R(t)$ for: (b) $\varepsilon = 0.052$, (c) $\varepsilon = 0.090$ with trajectories initialized in the synchronized (blue) and unsynchronized (cyan) basins, (d) $\varepsilon = 0.130$, (e) $\varepsilon = 0.300$, and (f) $\varepsilon = 0.500$. In panels (b)–(f), red shading highlights time intervals where $R(t) > 0.8$, indicating partial phase synchronization. (For interpretation of the references to color in this figure legend, the reader is referred to the web version of this article.)

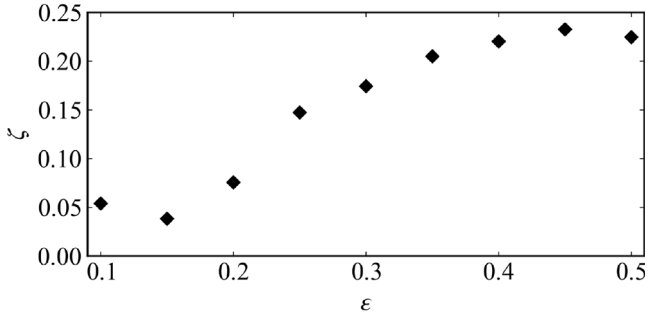


Fig. 4. Standard deviation (ζ) of the order parameter, computed from time series os each HR neuron of the network according to Eq. (7), as a function of the coupling strength ε. Increasing values of ζ with ε indicate a loss of stability of the phase-synchronized state.

neurons. Panels (b) and (d) clearly show fluctuations of $R(t)$ around values close to zero for the unsynchronized case (b), while panel (d) exhibits similar fluctuations, but around one, characterizing a partially phase-synchronized attractor. In panel (c), we show the two possible states of $R(t)$ within the bistable interval.

Note that both fluctuations around zero or near zero in panels (b), (c) and (d) of Fig. 3 are characterized by two distinct behaviors: a fluctuation with a mean that remains relatively constant over time, superimposed by random excursions up (down) in the values of the order parameter beyond its typical fluctuations.

Analyzing the results of panel (a) for values of the coupling strength larger than $\varepsilon = 0.115$, we observe that as the coupling strength increases, the average value of the order parameter $\langle R \rangle$ decreases. A combined analysis of $R(t)$ in panels (d)–(f) clarifies the reason for this decrease: as the coupling increases, $R(t)$ exhibits enhanced fluctuations. Note that with stronger coupling, the fluctuations around the expected value $R(t) = 1.0$ become more pronounced, indicating a loss of stability of the synchronized state. This loss of stability arises from the local dynamics of the attractor, since after being ejected from it, the trajectory repeatedly returns, showing that the attractor remains globally stable.

This mechanism of ejections followed by re injections into the synchronized state can be understood in terms of the scenario of Unstable Dimension Variability (UDV) of the attractor [34]. UDV is a phenomenon observed in strongly non hyperbolic chaotic

systems where the number of unstable directions, namely those associated with positive Lyapunov exponents, varies across the attractor [35]. In these situations, nearby trajectories to the attractor may experience different local instabilities, leading to fluctuations in the system's dimensionality of chaos [36–38]. This variability destroys uniform hyperbolicity, making the system highly sensitive to perturbations and often resulting in intermittent transitions between stable and unstable behavior. UDV typically occurs near transition points where different dynamical regimes coexist, as is the case in the hysteretic regime depicted by the network [39]. It gives rise to complex behaviors such as chaotic intermittency, loss of predictability, and riddled basin structures [40]. In our network dynamics, the presence of UDV often signals the onset of instability in the synchronized state, as trajectories intermittently depart from and return to the synchronization manifold [41].

The presence of UDV depends on finding coexisting sets in the chaotic invariant set of periodic orbits with different numbers of unstable directions. Rigorous proofs of this condition are quite difficult to perform in higher-dimensional systems, such as for coupled HR neurons, where the phase space has large dimensionality. A numerical verification of UDV is possible, though, with the help of finite-time Lyapunov exponents $\tilde{\lambda}_i(t)$. The latter are computed as usual Lyapunov exponents, but taking finite (and usually small) time intervals of length t.

A coupled system of N HR neurons has a $3N$-dimensional phase space, with a 3-dimensional synchronization manifold. The stability properties of the synchronized state are thus condensed in the $3(N-1)$ transversal Lyapunov exponents $\lambda_{T,i}$. Usually, the information about UDV is obtained from the maximal transversal exponent $\lambda_{T,max}$, but we will see that other transversal exponents are also worth investigating. The presence of UDV is thus related to the fluctuating behavior about zero of the maximal transversal time-t exponents $\tilde{\lambda}_{T,max}(t)$ [1]. This is because $\lambda_{T,max}$ is the closest exponent to zero and thus the presence of positive and negative fluctuations of time-t exponents reflects the alternating behavior between attracting and repelling behavior with respect to the synchronization manifold [42].

Whereas the infinite-time limit of the Lyapunov exponents is independent of the initial conditions, the time-T exponents $\tilde{\lambda}_{T,i}(t)$ depend on them. We use ergodicity to sample nonoverlapping sections of length t from a long chaotic trajectory of the system and compute the finite-time fluctuations $\tilde{\lambda}_{T,i}(t)$ for this trajectory, obtaining a probability distribution $P_i(\tilde{\lambda}_{T,i}(t))$ for each transversal exponent. The total probability distribution $\sigma(\tilde{\lambda}_{T,i}(t))$ is obtained by combining the distributions of all transversal exponents (not only the maximal one, although it conveys most of the statistical information). Hence, a fingerprint of UDV is the existence of both negative and positive fluctuations of $\sigma(\tilde{\lambda}_{T,i}(t))$ or, in particular, a nonzero positive fraction.

Fig. 4 shows the standard deviation ζ of the time series of $R(t)$ for $0.1 < \varepsilon < 0.5$. A pronounced increase in the amplitude of fluctuations can be seen just after the start of the stable phase-synchronized state. As the coupling increases, ζ approaches the expected standard deviation for uniformly distributed noise in the interval $[0, 1]$, namely $1/(2\sqrt{3})$, while the mean value still remains very close to 1, in contrast to the expected value of 0.5 for purely uniformly random fluctuations. Our conclusion in this case is that such fluctuations are due to trajectory escapes caused by unstable manifolds transverse to the phase-synchronized state. In this situation, the trajectory remains close to the synchronized manifold for a sufficiently long time so that the average value of the order parameter stays near one, but it undergoes ballistic escapes due to tangencies with unstable manifolds induced by the presence of UDV in the synchronized dynamics.

To test the hypothesis of UDV in the partially phase-synchronized state of the HR oscillator network, we computed the finite-time Lyapunov spectrum of the system for a trajectory in the parameter space of Fig. 1. This procedure yields 600 distributions of Lyapunov exponents. A subset of these exponents exhibits fluctuations around zero, indicating the possible presence of UDV in our system. To compute the fluctuations, a value of ± 0.001 was defined as the smallest value of exponent considered to be different from zero.

The set of distributions of all Lyapunov exponents exhibiting fluctuations around zero is shown in Fig. 5 for several coupling values. For low coupling strengths e.g. panel (a) $\varepsilon = 0.052$, where the dynamics are unsynchronized, a relatively weak UDV regime is observed. As the coupling increases, the system enters the hysteretic regime, as exemplified in Fig. 5 panels (b) for the lower branch state and (c) for the upper branch state of Fig. 5 and $\varepsilon = 0.090$. Clearly, the distributions exhibit two maxima one negative and one lightly positive, while the occurrence of values around zero is mildly suppressed. In this region, UDV is present again. Note that many negative Lyapunov exponents exhibit intermittent excursions into positive values. This feature of the exponent spectrum may be associated with the random fluctuations in the values of $R(t)$ shown in panels (b)–(d) of Fig. 3. This large number of negative exponents forces the system to return rapidly to its original state, preventing it from transitioning to a different asymptotic state. In this region, we say the characteristics of UDV allow the coexistence of two globally stable states with minimal influence from the local dynamics that can induce just small ejections from either state. For larger coupling values, panels (d)–(f) of Fig. 5, the presence of UDV becomes more pronounced. Increases in the coupling strength lead to larger values of the finite-time Lyapunov exponents as well as a large distribution of them. This behavior supports the fact that ejections from the partially synchronized state become progressively more intense, leading to increasingly frequent intervals where $R(t)$ attains very low values.

To further elucidate the role of UDV in the transition process from unsynchronized to phase-synchronized states in the network, panel (a) of Fig. 6 shows the average order parameter $\langle R \rangle$ computed for parameter values $b = 2.680$, $I = 4.280$ corresponding to the lower red bullet in the parameter space shown in Fig. 1(a), namely one that does not exhibit hysteresis but rather an interval of coupling strengths for which synchronized states occur intermittently.

Similarly to Fig. 3, panels (b) and (d)–(f) of Fig. 6 also show that the network behavior for low and high values of the coupling parameter does not change qualitatively. However, panel (c) of Fig. 6 clearly shows that the hysteresis region observed in Fig. 3 panel (c) now exhibits intermittent behavior. In this case, both the unsynchronized and the phase-synchronized attractors are no longer globally stable and thus do not possess individual basins of attraction. Instead, an intermittent dynamics is observed, suggesting the

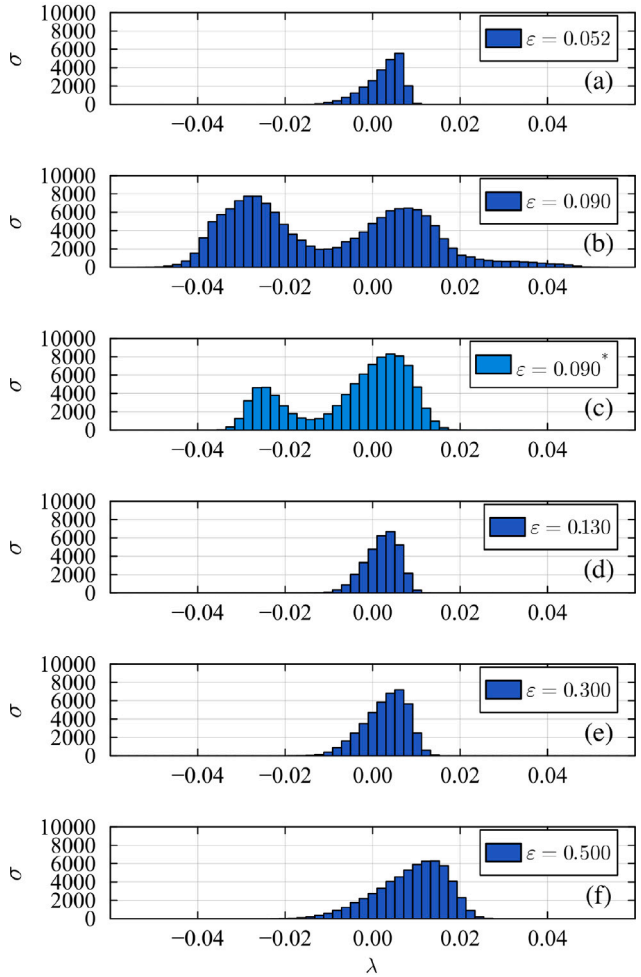


Fig. 5. Histogram of all finite time Lyapunov exponent (t = 300) that oscillate around zero, for b = 2.660, I = 4.325 and coupling strength parameter (a) ε = 0.052, (b) ε = 0.076 synchronized state (blue), (c) ε = 0.099 unsynchronized state (cyan), (d) ε = 0.130, (e) ε = 0.300, (f) ε = 0.500. (For interpretation of the references to color in this figure legend, the reader is referred to the web version of this article.)

presence of two regions in phase space where the local dynamics, influenced by unstable directions, prevent the trajectory from remaining there, thereby leading the system to exhibit an intermittent regime.

To better understand the reasons why the hysteresis region of the network was replaced by an intermittent transition from the unsynchronized to the phase-synchronized state, Fig. 7, similarly to Fig. 5, presents the distributions of all Lyapunov exponents of the network that fluctuate around zero. An examination of panel (b) in Fig. 7 shows that the bimodal distribution observed in the hysteresis region of the network, as shown in Fig. 5, is now replaced by a uni modal distribution centered at values close to zero. It is observed that the portion of the bimodal distribution corresponding to negative exponents with excursions into positive values (left part of the distribution) is completely suppressed, whereas the distribution of positive exponents with excursions into negative values undergoes little change. This behavior reinforces the dominance of UDV, completely inhibiting the possibility of remaining in either the phase-synchronized or the unsynchronized states due to the presence of strong unstable directions imposed by the UDV. This scenario suppresses the coexistence of two globally stable states. We say that a stronger presence of UDV enhances the role of the local dynamics, making it more susceptible to destabilization through unstable manifolds induced by UDV. As a result, the system no longer remains in either of the two states but instead alternates intermittently between two regions of the phase space.

In this situation, the unsynchronized state begins to lose stability, it is like an "inverse" blowout bifurcation scenario [36–38], where the transverse stability of the manifold is lost, giving rise to laminar phases in which the network exhibits partial phase synchronization, configuring a UDV onset of synchronization in a network where the oscillators may exhibit on–off intermittency, characterized by long laminar intervals of near-unynchronization punctuated by irregular bursts of partial phase synchronization. To quantify this regime, we analyze the distribution of mean laminar-phase durations, namely intervals during which the global order parameter remains below a prescribed threshold ($R_{\text{th}} = 0.5$). Our results are plotted in Fig. 8. The mean duration of these laminar intervals follows a two-stage statistical fitting procedure: For long laminar phases, occurring for coupling just above $\varepsilon_c = 0.060$, the

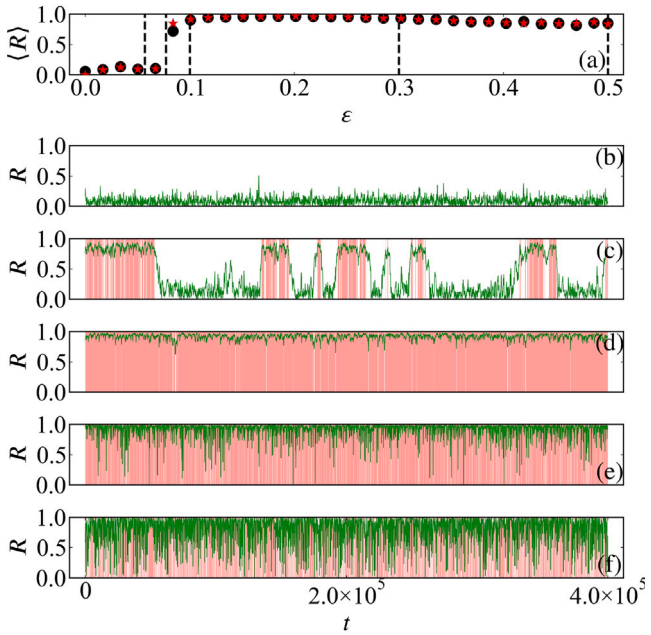


Fig. 6. (a) Mean Kuramoto order parameter $\langle R \rangle$ as a function of the coupling strength ε for $b = 2.680$ and $I = 4.280$, obtained using continuation. Black dots correspond to the forward continuation, while red stars denote the backward continuation. Vertical dashed lines mark the coupling values used in panels (b)–(f). Panels (b)–(f) show the time series of the Kuramoto order parameter $R(t)$ for: (b) $\varepsilon = 0.052$, (c) $\varepsilon = 0.076$, (d) $\varepsilon = 0.099$, (e) $\varepsilon = 0.300$, (f) $\varepsilon = 0.500$. In panels (b)–(f), red shading highlights time intervals where $R(t) > 0.8$, indicating partial phase synchronization. (For interpretation of the references to color in this figure legend, the reader is referred to the web version of this article.)

distribution follows a power-law decay (blue curve)

$$\tau \sim A(\varepsilon - \varepsilon_c)^{-\alpha},$$

consistent with the universal scaling predicted for systems near a blowout or transverse Lyapunov instability under multiplicative fluctuations. Here, $A \sim 403134$ and $\alpha \sim -0.15$. Deviations from the pure power law arise for $\varepsilon \gg \varepsilon_c$, where the probability density exhibits an exponential cutoff, configuring a heavy-tailed distribution. Note that for values well above the onset of synchronization threshold ε_c, this heavy-tailed effect becomes more pronounced, causing laminar periods even shorter than those predicted by the single exponential approximation to lose validity. This characteristic is likely due to the continuous variation in the degree of UDV and the presence of a partially synchronized manifold. In this case

$$\tau \sim A(\varepsilon - \varepsilon_c)^{-\alpha} \exp\left[-\beta(\varepsilon - \varepsilon_c)\right],$$

for $\beta \sim -163$ reflecting the finite probability that noise or fluctuating coupling drives the system back into a synchronized burst (red line in Fig. 8).

Fitting the data separately in these two regimes provides a sensitive diagnostic of proximity to the synchronization transition, allowing the combined power-law plus exponential model to serve as a quantitative marker of how intermittency scales near the onset of collective synchronization.

In general, the importance and relevance of UDV in transition processes can be summarized by computing the area of the histograms shown in Figs. 5 and 7. The area of the Lyapunov exponent histogram in a neighborhood of zero provides a useful quantitative indicator UDV. A significant concentration of histogram weight near zero indicates frequent transitions between locally stable and unstable dynamics, signaling strong UDV that is maximized if the negative and positive areas are equal, resulting in a null area. Conversely, if the distribution is well separated from zero, the system tends to have a more uniform hyperbolic structure with a fixed number of unstable directions. Thus, the integrated area of exponents that fluctuates around zero serves as a practical diagnostic [39,40]: small values correspond to enhanced variability in the local dimensionality of instability, while larger values suggest more stable dynamical behavior. To quantify the role of UDV in the transition to phase-syncronized states, Fig. 9 shows the values of the area for all Lyapunov exponents that fluctuate around zero. As can be observed, in the hysteresis region, this area is significantly larger, indicating a weaker UDV effect.

4. Conclusions

In general, the transition towards synchronized states in the Hindmarsh–Rose (HR) model is expected to follow a well-known scenario when coupling strength increases [8]: uncoupled chaotic neurons gradually become more synchronized as the coupling

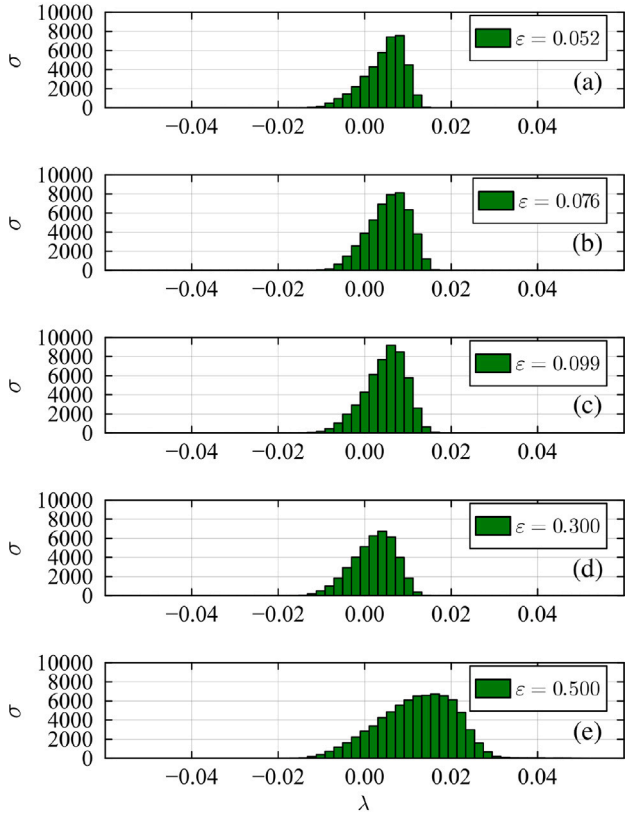


Fig. 7. Histogram of all finite time Lyapunov exponent ($t = 300$) that oscillate around zero, for $b = 2.680$ and $I = 4.280$ with strength coupling parameter (a) $\varepsilon = 0.052$, (b) $\varepsilon = 0.076$, (c) $\varepsilon = 0.099$, (d) $\varepsilon = 0.300$, (e) $\varepsilon = 0.500$. (For interpretation of the references to color in this figure legend, the reader is referred to the web version of this article.)

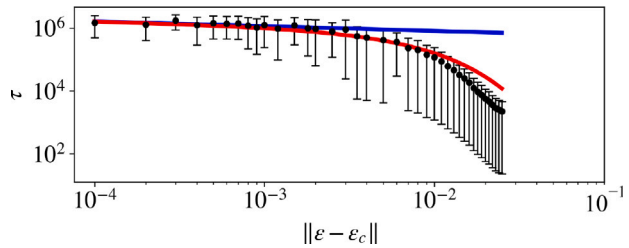


Fig. 8. Distribution of laminar-phase durations during the UDV induced onset of synchronization, resembling a on-off intermittent synchronization of the network. The data (dots) show the probability density $P(\tau)$ of laminar intervals, revealing a power-law regime for short durations (blue curve) followed by an exponential cutoff for long durations (red curve). The solid line represents the fit to the scaling law $\tau \sim A(\varepsilon - \varepsilon_c)^{-\alpha}$ in the power-law region, while the dashed line shows the full power-law-plus-exponential model $\tau \sim A(\varepsilon - \varepsilon_c)^{-\alpha} \exp\left[-\beta(\varepsilon - \varepsilon_c)\right]$ capturing the tail behavior. This combined fitting demonstrates the characteristic signature of on–off intermittency near the synchronization transition. Bullets represent the mean values obtained from 30 simulations, while the error bars indicate the standard deviation of the mean. (For interpretation of the references to color in this figure legend, the reader is referred to the web version of this article.)

strength grows, and once a critical threshold is surpassed, the network starts to shift from an unsynchronized chaotic state to a phasesynchronized one.

However, the transition is strongly dependent on the individual dynamics of the neurons and on parameter-space values that influence the emergence of different transition mechanisms, even for subtly different parameters.

For intermixed regions of the parameter space shown as colored areas in Fig. 1, this transition may display either two coexisting stable states or intermittent states.

The coexisting states give rise to hysteretic behavior in which synchronized and unsynchronized network dynamics coexist. In this scenario, explosive synchronization mechanisms may occur [10,16], arising from the subtle loss of stability of the unsynchronized state.

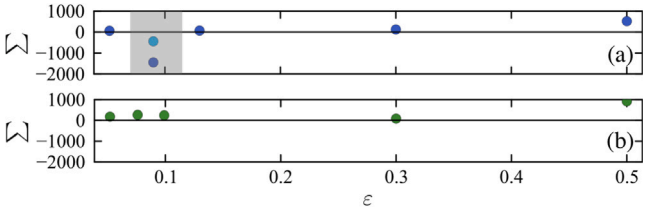


Fig. 9. Computed areas ($\sum$) of all histogram plotted in Fig. 5, panel (a) and Fig. 7, panel (b) as a function os the coupling strength. Clearly, these areas increase in the transition region to phase-synchronized states that involve states with hysteresis (gray shaded area in panel (a)). Since areas close to zero indicate a maximum in UDV intensity, these results can be interpreted as a decrease in UDV intensity during the transition in the presence of hysteresis. The dark blue and cyan bullets inside the gray shaded hysteresis area correspond, respectively, to the two hysteresis branches shown in Fig. 5. (For interpretation of the references to color in this figure legend, the reader is referred to the web version of this article.)

The intermittent states are intermixed with the hysteresis and result in a completely different scenario for the transition to phase synchronized states.

Here, we present results for two representative pairs of parameter sets sampled from the colored (chaotic) regions of Fig. 1, each illustrating one of the two types of behavior: the presence of two stable states with a hysteretic transition, and the intermittent transition. Based on additional simulations, we find that both behaviors are observed over a wide parameter region within the chaotic regimes shown in color in Fig. 1.

Here, we show that these two possible transitions are strongly linked to the presence of different levels and characteristics of UDV in the network dynamics.

We have shown that moderate levels of unstable dimension variability (UDV) allow the coexistence of two stable network states: one unsynchronized and one synchronized. Under these conditions, the network can alternate between two globally stable modes of activity. In contrast, other regions of the parameter space exhibit stronger UDV, which disrupts the global stability of both states. In these cases, the attractor displays spatially heterogeneous stability, meaning that the degree of stability varies across different regions of the network trajectory within the attractor.

As the coupling strength continues to increase, even for values much greater than the critical values for phase synchronization, the UDV mechanism enhances the variability of the stable dimension of the synchronization manifold, eventually destroying completely the hysteresis scenario.

Due to the loss of stability of both synchronized and unsynchronized states, the hysteretic regime is replaced by an intermittent one. These two regimes are associated with markedly different levels of unstable dimension variability (UDV), with the intermittent regime exhibiting a significantly stronger degree of UDV.

Finally, we believe that the analysis carried out here for a particular model may be replicated in many others, making UDV a mechanism that should be taken into account in transition processes in other coupled network models.

CRediT authorship contribution statement

Emanuel Barbosa Sant Anna Cambraia: Writing – original draft, Visualization, Validation, Software, Methodology, Investigation, Formal analysis, Data curation, Conceptualization. **Thiago Lima Prado:** Methodology, Investigation, Formal analysis, Data curation. **Ricardo Luiz Viana:** Methodology, Investigation, Formal analysis, Data curation, Conceptualization. **Sergio Roberto Lopes:** Writing – review & editing, Writing – original draft, Validation, Supervision, Project administration, Methodology, Funding acquisition, Formal analysis, Conceptualization.

Declaration of competing interest

The authors declare that they have no known competing financial interests or personal relationships that could have appeared to influence the work reported in this paper.

Acknowledgments

This study was financed by the Coordenação de Aperfeiçoamento de Pessoal de Nível Superior, Brazil (CAPES), Finance Code 001; Conselho Nacional de Desenvolvimento Científico e Tecnológico, CNPq, Brazil through grant Numbers 88887.885821/2023-00, 88887.798757/2022-00, 308441/2021-4, 403120/2021-7, and 308621/2019-0; This research is also supported by INCT-NeuroComp (CNPq) Grant 408389/2024-9 and Financiadora de Estudos e Projetos (FINEP), Brazil. Computer simulations were performed at the LCPAD-CTINFRA cluster at Universidade Federal do Paraná.

Data availability

Data will be made available on request.

References

[1] Dayan P, Abbott LF. Theoretical neuroscience: computational and mathematical modeling of neural systems. Cambridge, MA: MIT Press; 2001.
[2] Kandel ER, Schwartz JH, Jessell TM, Siegelbaum SA, Hudspeth AJ. Principles of neural science. Vol. 4, McGraw-Hill; 2000.
[3] Boccaletti S, Latora V, Moreno Y, Chavez M, Hwang D-U. Complex networks: Structure and dynamics. Phys Rep 2006;424(4–5):175–308. http://dx.doi.org/10.1016/j.physrep.2005.10.009.
[4] Izhikevich EM. Dynamical systems in neuroscience. MIT Press; 2007.
[5] Fell J, Axmacher N. The role of phase synchronization in memory processes. Nature Rev Neurosci 2011;12(2):105–18. http://dx.doi.org/10.1038/nrn2979.
[6] Kandel ER. The molecular biology of memory storage: A dialogue between genes and synapses. Science 2001;294(5544):1030–8. http://dx.doi.org/10.1126/science.1067020.
[7] Gerstner W, Kistler WM, Naud R, Paninski L. Neuronal dynamics: From single neurons to networks and models of cognition. Cambridge, UK: Cambridge University Press; 2014.
[8] Pikovsky AS, Rosenblum MG, Kurths J. Synchronization: A universal concept in nonlinear sciences. Vol. 12, Cambridge University Press; 2003.
[9] Pikovsky AS, Rosenblum MG, Osipov GV, Kurths J. Phase synchronization of chaotic oscillators by external driving. Phys D 1997;104(3–4):219–38.
[10] Arenas A, Díaz-Guilera A, Kurths J, Moreno Y, Zhou C. Synchronization in complex networks. Phys Rep 2008;469(3):93–153. http://dx.doi.org/10.1016/j.physrep.2008.09.002.
[11] Hodgkin AL, Huxley AF. A quantitative description of membrane current and its application to conduction and excitation in nerve. J Physiol 1952;117(4):500–44.
[12] Hindmarsh JL, Rose RM. A model of neuronal bursting using three coupled first order differential equations. Proc R Soc Lond Ser B. Biological Sci 1984;221(1222):87–102.
[13] Destexhe A, Mainen ZF, Sejnowski TJ. An efficient method for computing synaptic conductances based on a kinetic model of receptor binding. Neural Comput 1994;6(1):14–8.
[14] Rosenblum MG, Pikovsky AS, Kurths J. Synchronization approach to analysis of biological systems. Fluct Noise Lett 2004;4(01):L53–62.
[15] Rosenblum MG, Pikovsky AS, Kurths J. Phase synchronization of chaotic oscillators. Phys Rev Lett 1996;76(11):1804.
[16] Boaretto BRR, Manchein C, Prado TL, Lopes SR. The role of individual neuron ion conductances in the synchronization processes of neuron networks. Neural Netw 2021;137:97–105. http://dx.doi.org/10.1016/j.neunet.2021.01.019.
[17] Boaretto BRR, Budzinski RC, Prado TL, Kurths J, Lopes SR. Suppression of anomalous synchronization and nonstationary behavior of neural network under small-world topology. Phys A 2018;497:126–38.
[18] Boaretto BRR, Budzinski RC, Prado TL, Lopes SR. Mechanism for explosive synchronization of neural networks. Phys Rev E 2019;100(5):052301.
[19] Cambraia EBSA, Flauzino JVV, Prado TL, Lopes SR. Dependence on the local dynamics of a network phase synchronization process. Phys A 2023;619:128750. http://dx.doi.org/10.1016/j.physa.2023.128750.
[20] Uhlhaas PJ, Singer W. Neural synchrony in brain disorders: Relevance for cognitive dysfunctions and pathophysiology. Neuron 2006;52(1):155–68. http://dx.doi.org/10.1016/j.neuron.2006.09.020.
[21] Little S, Brown P. What brain signals are suitable for feedback control of deep brain stimulation in Parkinson's disease? Ann New York Acad Sci 2012;1265(1):9–24. http://dx.doi.org/10.1111/j.1749-6632.2012.06650.x.
[22] Uhlhaas PJ, Singer W. Abnormal neural oscillations and synchrony in schizophrenia. Nature Rev Neurosci 2010;11(2):100–13. http://dx.doi.org/10.1038/nrn2774.
[23] Ji P, Peron TKD, Menck PJ, Rodrigues FA, Kurths J. Cluster explosive synchronization in complex networks. Phys Rev Lett 2013;110:218701. http://dx.doi.org/10.1103/PhysRevLett.110.218701.
[24] Kuramoto Y. Cooperative dynamics of oscillator communitya study based on lattice of rings. Progr Theoret Phys Suppl 1984;79:223–40.
[25] Kuramoto Y. Chemical oscillations, waves, and turbulence. Vol. 19, Springer Science & Business Media; 2012.
[26] de Lange E, Hasler M. Predicting single spikes and spike patterns with the Hindmarsh–Rose model. Biol Cybernet 2008;99(4):349–60. http://dx.doi.org/10.1007/s00422-008-0260-y.
[27] Barrio R, Angeles Martínez M, Serrano S, Shilnikov A. Macro- and micro-chaotic structures in the Hindmarsh-Rose model of bursting neurons. Chaos: An Interdiscip J Nonlinear Sci 2014;24(2):023128. http://dx.doi.org/10.1063/1.4882171.
[28] Gu H. Biological experimental observations of an unnoticed chaos as simulated by the Hindmarsh-Rose model. PLoS One 2013;8(12):1–12. http://dx.doi.org/10.1371/journal.pone.0081759.
[29] Malik S, Mir A. Synchronization of Hindmarsh Rose neurons. Neural Netw 2020;123:372–80. http://dx.doi.org/10.1016/j.neunet.2019.11.024.
[30] Innocenti G, Genesio R. On the dynamics of chaotic spiking-bursting transition in the Hindmarsh–Rose neuron. Chaos: An Interdiscip J Nonlinear Sci 2009;19(2):023124. http://dx.doi.org/10.1063/1.3156650.
[31] Wolf A, Swift JB, Swinney HL, Vastano JA. Determining Lyapunov exponents from a time series. Phys D 1985;16(3):285–317.
[32] Ivanchenko MV, Osipov GV, Shalfeev VD, Kurths J. Phase synchronization in ensembles of bursting oscillators. Phys Rev Lett 2004;93(13):134101.
[33] van Hemmen JL, Wreszinski WF. Lyapunov function for the Kuramoto model of nonlinearly coupled oscillators. J Stat Phys 1993;72(1):145–66. http://dx.doi.org/10.1007/BF01048044.
[34] Dawson SP, Grebogi C, Sauer T, Yorke JA. Obstruction to shadowing when a Lyapunov exponent fluctuates about zero. Phys Rev Lett 1994;73(14):1927–30. http://dx.doi.org/10.1103/PhysRevLett.73.1927.
[35] Abraham R, Smale S. Nongenericity of Ω-stability. In: Proceedings of symposia in pure mathematics. Vol. 14, American Mathematical Society; 1970, p. 5–8.
[36] Lai Y-C, Grebogi C, Yorke JA, Venkataramani SC. Riddled basins in chaotic dynamical systems. Phys Rev Lett 1996;77(1):55–8. http://dx.doi.org/10.1103/PhysRevLett.77.55.
[37] Lai Y-C, Grebogi C, Yorke JA. Unstable dimension variability in coupled chaotic systems. Phys Rev Lett 1997;79(1):65–8. http://dx.doi.org/10.1103/PhysRevLett.79.65.
[38] Viana RL, Grebogi C. Unstable dimension variability and synchronization of chaotic systems. Phys Rev E 2000;62(1):462.
[39] Viana RL, Grebogi C, de S. Pinto SE, Lopes SR, Batista AM, Kurths J. Validity of numerical trajectories in the synchronization transition of complex systems. Phys Rev E 2003;68(6):067204. http://dx.doi.org/10.1103/PhysRevE.68.067204.
[40] Viana RL, Grebogi C, de S. Pinto SE, Lopes SR, Batista AM, Kurths J. Bubbling bifurcations: Loss of synchronization and shadowing breakdown in complex systems. Phys D 2005;206:94–110. http://dx.doi.org/10.1016/j.physd.2005.05.005.
[41] Viana RL, Pinto SES, Grebogi C. Scaling laws for chaotic saddles in weakly dissipative systems. Phys Rev E 2002;66:046213. http://dx.doi.org/10.1103/PhysRevE.66.046213.
[42] Kostelich EJ, Kan I, Grebogi C, Ott E, Yorke JA. Unstable dimension variability: An introduction. Phys D 1997;109(1–2):81–90. http://dx.doi.org/10.1016/S0167-2789(97)00151-7.